COBEM 2021 26th International Congress of Mechanical Engineering
November 22-26, 2021, Virtual Congress, Brazil

COB-2021-1329
Non-linear Finite Element Method Analysis applied to Functionally Graded Timoshenko Beams

Marcos Antonio Riquetto Ezequiel
Departamento de Mecânica Computacional, UNICAMP, Rua Mendeleyev 200, 13083-860, Cidade Universitária - Campinas, Brazil
m221513@dac.unicamp.br

Carlos Henrique Daros
Departamento de Mecânica Computacional, UNICAMP, Rua Mendeleyev 200, 13083-860, Cidade Universitária - Campinas, Brazil
chdaros@fem.unicamp.br

Abstract. *A non-linear finite element analysis is considered here for the static modelling of Functionally Graded Material (FGM) Timoshenko beams. FGMs play a key role in advanced tailored multifunctional materials. An example of FGMs are metal-ceramic composites used in the aerospace industry. We consider here a geometric nonlinearity for the beams in the form of small strains and moderate rotations. Non-homogeneity is considered along the beam's height. As a result of the non-homogeneity, we have additionally to the axial and bending stiffnesses the presence of an axial-bending coupling stiffness. Different material law distributions along the beam's height will be investigated as power-law and exponential-law distributions. The stresses will be equally assessed to optimize the beams' performances for the different material law distributions and different boundary conditions. The axial bending coupling, which is partly inherent to the geometric non-linearity of the beam, modeled here via finite elements, may produce membrane locking effects. Reduced integration will be applied to circumvent such membrane locking effects.*

Keywords: *Non-Linear Finite Element Analysis, Functionally graded materials, Timoshenko beam.*

1. INTRODUCTION

Structural computational linear analysis is a powerful method to assess the behavior of complex structures. However linear formulation has its limitations. In the beam formulations this limitations can be of geometrical and/or material nature. When the applied loads on beam are large the linear load-deflection behavior no longer occurs, since the beam starts to develop internal forces that resist deformation, the larger the loading and deformation the larger this internal forces become (Reddy, 2014). This means that the nonlinear analysis will result in a more rigid beam and allow for greater loads, because the nonlinear analyses represents better the beam's behavior.

The classical Euler-Bernoulli beam theory does not include the effects of the shear deformation, for chubby beams the shear stress cannot be neglected (Shames and Dym, 2013). In order to generalize the beam formulation the Timoshenko beam theory was used, in general the shear strain begins to be relevant at length-to-height ratios less than 25 (Reddy, 2014).

Geometric nonlinearity and Timoshenko beam theory allow a more realistic modelling of beams. However, geometric non-linear analysis and the inclusion of shear deformation may present some numerical difficulties known as locking effects. The locking effects for beams are associated with shear and membrane locking. Reduced numerical integration is a common way to circumvent such numerical difficulties.

Timoshenko Beams allow us to investigate here the behaviour of some functionally graded materials (FGMs). FGMs are advanced tailored multifunctional materials which have several key applications, such as in the aerospace industry (Mortsen and Suresh, 1998).

2. FORMULATION

The Non-linear Timoshenko Finite Element utilized in this paper is based on the formulation presented by Reddy (2014), which takes into account small strains and small to moderate rotations. So the geometric nonlinearity of the problem is originated by the inclusion of square terms of the rotation while neglecting square terms of in plane stretching, known as the *von Kármán nonlinearity*. It is also assumed that in view of the small strain, it is not necessary to distinguish between deformed and undeformed coordinates.

2.1 Timoshenko beam

The classical Euler Bernoulli beam theory states that a plane section perpendicular to the main axis of a beam in the undeformed state remains plane and normal to the axis as the beam bends from loads (Shames and Dym, 2013). This is equivalent to neglecting the Poisson effect and transverse and shear strain terms. The Timoshenko beam theory uses similar assumptions, however the plane sections no longer need to be normal to the main axis, this enables the appearance of shear strains on the beam.

The Figure (1) represents the Kinematics of the Timoshenko theory, from them the displacement field of a Timoshenko

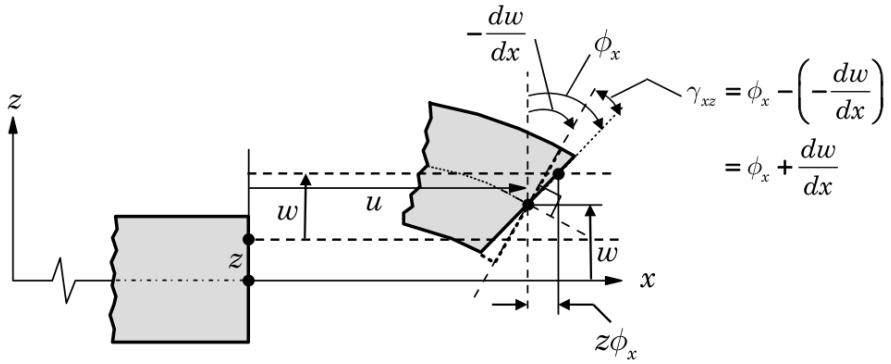

Figure 1. Kinematics of a beam in the Timoshenko beam theory (Reddy, 2014).

beam can be expressed as

$$u_1 = u(x) + z\phi_x(x), \quad u_2 = 0, \quad u_3 = w(x) \tag{1}$$

where (u_1, u_2, u_3) are the total displacements of a material on the (x, y, z) coordinates, u, w are the axial and transverse displacements relative to the x-axis, situated along the geometric centroid of the cross section of the beam and ϕ_x is the rotation, about the y axis of the transverse plane. From the displacement field we can write the only non-zero strain terms, the axial strain ε_{xx} and shear strain γ_{xz} as

$$\varepsilon_{xx} = \frac{\partial u_1}{\partial x} + \frac{1}{2}\left(\frac{\partial u_3}{\partial x}\right)^2 = \frac{du}{dx} + \frac{1}{2}\left(\frac{dw}{dx}\right)^2 + z\frac{d\phi_x}{dx} \equiv \varepsilon^0_{xx} + z\varepsilon^1_{xx} \tag{2}$$

$$\gamma_{xz} = \frac{\partial u_1}{\partial z} + \frac{\partial u_3}{\partial x} = \phi_x + \frac{dw}{dx} \equiv \gamma^0_{xz} \tag{3}$$

Through the principle of virtual displacement we are able to build the weak form of the problem. For an element in the domain $\Omega_e = (x_a, x_b)$, the total virtual work δW^e can be expressed as

$$0 = \delta W^e \equiv \delta W^e_I + \delta W^e_E \tag{4}$$

The virtual strain energy δW^e_I and work done by external forces δW^e_E are given by

$$\delta W^e_I = \int_{x_a}^{x_b}\int_{A^e} \left(\sigma_{xx}\delta\varepsilon_{xx} + \sigma_{xz}\delta\gamma_{xz}\right) dAdx = \int_{x_a}^{x_b} \left(N_{xx}\delta\varepsilon^0_{xx} + M_{xx}\delta\varepsilon^1_{xx} + Q_x\delta\gamma^0_{xz}\right) dx \tag{5}$$

$$\delta W^e_E = -\left[\int_{x_a}^{x_b} q\delta w dx + \int_{x_a}^{x_b} f\delta u dx + \sum_{i=1}^{6} Q^e_i\delta\Delta^e_i\right] \tag{6}$$

where σ_{xx} is the axial stress, σ_{xz} is the shear stress, A^e is the element cross sectional area, N_{xx} is the axial force, Q_x is the shear force, M_{xx} is the bending moment, f and q are the axial and transverse distributed loads, $Q^e_i (i = 1 : 6)$ are the element generalized forces and $\Delta^e_i (i = 1 : 6)$ are the element generalized displacements. From Equations (5) and (6)

$$N_{xx} = \int_A \sigma_{xx} dA, \quad M_{xx} = \int_A \sigma_{xx} z dA, \quad Q_x = \int_A \sigma_{xz} dA, \quad \sigma_{xx} = E\varepsilon_{xx}, \quad \sigma_{xz} = K_s G\gamma_{xz} \tag{7}$$

here E is the modulus of elasticity, G is the shear modulus and K_s is the shear correction coefficient. The correction coefficient appears to account for the difference between the constant shear stress through the beam thickness, predicted by the Timoshenko beam theory and the parabolic variation predicted by the elasticity theory (Reddy, 2006).

The axial and shear forces and bending moment can be rewritten in terms of the generalized displacements using Equations (2),(3) and (7)

$$N_{xx} = A_{xx}\left[\frac{du}{dx} + \frac{1}{2}\left(\frac{dw}{dx}\right)^2\right] + B_{xx}\frac{d\phi_x}{dx}, \quad M_{xx} = B_{xx}\left[\frac{du}{dx} + \frac{1}{2}\left(\frac{dw}{dx}\right)^2\right] + D_{xx}\frac{d\phi_x}{dx} \tag{8}$$

$$Q_x = S_{xx}\left(\frac{dw}{dx} + \phi_x\right) \tag{9}$$

where A_{xx}, B_{xx}, D_{xx} and S_{xx} are the extensional, extensional-bending, bending and shear stiffnesses of the beam element

$$(A_{xx},\ B_{xx},\ D_{xx},\ S_{xx}) = \int_{A^e} E(x,z)\left(1, z, z^2, \frac{Ks}{2(1+\nu)}\right) dA \tag{10}$$

on beams with constant $E(x)$ through its thickness the extensional-bending stiffness is 0, since our interest is on beams with functionally graded materials this term will be non-zero.

The equilibrium equations of the Timoshenko Beam Theory are then given by

$$-\frac{d}{dx}\left\{A_{xx}\left[\frac{du}{dx} + \frac{1}{2}\left(\frac{dw}{dx}\right)^2\right] + B_{xx}\frac{d\phi_x}{dx}\right\} = f \tag{11}$$

$$-\frac{d}{dx}\left\{A_{xx}\frac{dw}{dx}\left[\frac{du}{dx} + \frac{1}{2}\left(\frac{dw}{dx}\right)^2\right] + B_{xx}\frac{dw}{dx}\frac{d\phi_x}{dx}\right\} - \frac{d}{dx}\left[S_{xx}\left(\frac{dw}{dx} + \phi_x\right)\right] = q \tag{12}$$

$$-\frac{d}{dx}\left\{D_{xx}\frac{d\phi_x}{dx} + B_{xx}\left[\frac{du}{dx} + \frac{1}{2}\left(\frac{dw}{dx}\right)^2\right]\right\} + S_{xx}\left(\frac{dw}{dx} + \phi_x\right) = 0 \tag{13}$$

From Eqs. (11), (12) and (13) it is possible to identify the coupling of the axial and transverse displacements caused by the *vón Kármán nonlinearity*, and also a coupling of the axial and transverse displacement and rotation caused by the extensional-bending stiffness originated from the material composition.

2.2 Finite Element

The finite element can be constructed using the virtual work Equation (4), which is equivalent to the Equations (14), (15) and (16):

$$0 = \int_{x_a}^{x_b}\left\{A_{xx}\frac{d\delta u}{dx}\left[\frac{du}{dx} + \frac{1}{2}\left(\frac{dw}{dx}\right)^2\right] + B_{xx}\frac{d\delta u}{dx}\frac{d\phi_x}{dx} - f\delta u\right\}dx - Q_1^e\delta u\left(x_a\right) - Q_4^e\delta u\left(x_b\right) \tag{14}$$

$$\begin{aligned} 0 = \int_{x_a}^{x_b}\frac{d\delta w}{dx}\left\{S_{xx}\left(\frac{dw}{dx} + \phi_x\right) + A_{xx}\frac{dw}{dx}\left[\frac{du}{dx} + \frac{1}{2}\left(\frac{dw}{dx}\right)^2\right] + B_{xx}\frac{dw}{dx}\frac{d\phi_x}{dx}\right\}dx \\ - \int_{x_a}^{x_b}\delta w q dx - Q_2^e\delta w\left(x_a\right) - Q_5^e\delta w\left(x_b\right) \end{aligned} \tag{15}$$

$$\begin{aligned} 0 = \int_{x_a}^{x_b}\left\{D_{xx}\frac{d\delta\phi_x}{dx}\frac{d\phi_x}{dx} + B_{xx}\frac{d\delta\phi_x}{dx}\left[\frac{du}{dx} + \frac{1}{2}\left(\frac{dw}{dx}\right)^2\right] + S_{xx}\delta\phi_x\left(\frac{dw}{dx} + \phi_x\right)\right\}dx \\ - Q_3^e\delta\phi_x\left(x_a\right) - Q_6^e\delta\phi_x\left(x_b\right) \end{aligned} \tag{16}$$

where δu, δw and $\delta\phi_x$ are the virtual displacements, which are equivalent to the weight functions in the Ritz-Galerkin model. The generalized forces Q_1^e, Q_4^e represent external axial forces, Q_2^e, Q_5^e represent external shear forces and Q_3^e, Q_6^e represent external moments, and can be written in relation to the axial displacement u, transverse displacement w and rotation ϕ_x as:

$$Q_1^e = -N_{xx}\left(x_a\right), \quad Q_4^e = N_{xx}\left(x_b\right), \quad Q_2^e = -\left[Q_x + N_{xx}\frac{dw}{dx}\right]_{x=x_a} \tag{17}$$

$$Q_5^e = \left[Q_x + N_{xx}\frac{dw}{dx}\right]_{x=x_b}, \quad Q_3^e = -M_{xx}\left(x_a\right), \quad Q_6^e = M_{xx}\left(x_b\right) \tag{18}$$

The virtual displacement terms in Equations (14), (15) and (16) show us that the $u(x)$, $w(x)$ and $\phi_x(x)$ are the primary variables and can be used as nodal degrees of freedom. The displacements are then expressed by

$$u(x) = \sum_{j=1}^{m} u_j^e \psi_j^{(1)}, \quad w(x) = \sum_{j=1}^{n} w_j^e \psi_j^{(2)}, \quad \phi_x(x) = \sum_{j=1}^{p} s_j^e \psi_j^{(3)} \tag{19}$$

where $\psi_j^{\alpha}(x)(\alpha = 1, 2, 3)$ are Lagrange interpolation functions of arbitrary degree. Now that we have an approximation of the displacement terms given by Eq. (19) we can substitute these terms on Equations (14), (15) and (16) and the virtual displacement terms $\delta u = \psi_i^{(1)}$, $\delta w = \psi_i^{(2)}$ and $\delta\phi_x = \psi_i^{(3)}$ to build the finite element model:

$$\begin{bmatrix} \mathbf{K}^{11} & \mathbf{K}^{12} & \mathbf{K}^{13} \\ \mathbf{K}^{21} & \mathbf{K}^{22} & \mathbf{K}^{23} \\ \mathbf{K}^{31} & \mathbf{K}^{32} & \mathbf{K}^{33} \end{bmatrix} \begin{Bmatrix} \mathbf{u} \\ \mathbf{w} \\ \mathbf{s} \end{Bmatrix} = \begin{Bmatrix} \mathbf{F}^1 \\ \mathbf{F}^2 \\ \mathbf{F}^3 \end{Bmatrix} \tag{20}$$

in which the stiffness coefficients are

$$K_{ij}^{11} = \int_{x_a}^{x_b} A_{xx} \frac{d\psi_i^{(1)}}{dx} \frac{d\psi_j^{(1)}}{dx} dx, \quad K_{ij}^{13} = \int_{x_a}^{x_b} B_{xx} \frac{d\psi_i^{(1)}}{dx} \frac{d\psi_j^{(3)}}{dx} dx = K_{ji}^{31} \tag{21}$$

$$K_{ij}^{12} = \frac{1}{2} \int_{x_a}^{x_b} A_{xx} \frac{dw}{dx} \frac{d\psi_i^{(1)}}{dx} \frac{d\psi_j^{(2)}}{dx} dx, \quad K_{ij}^{21} = \int_{x_a}^{x_b} A_{xx} \frac{dw}{dx} \frac{d\psi_i^{(2)}}{dx} \frac{d\psi_j^{(1)}}{dx} dx \tag{22}$$

$$K_{ij}^{22} = \int_{x_a}^{x_b} S_{xx} \frac{d\psi_i^{(2)}}{dx} \frac{d\psi_j^{(2)}}{dx} dx + \frac{1}{2} \int_{x_a}^{x_b} A_{xx} \left(\frac{dw}{dx} \right)^2 \frac{d\psi_i^{(2)}}{dx} \frac{d\psi_j^{(2)}}{dx} dx \tag{23}$$

$$K_{ij}^{23} = \int_{x_a}^{x_b} \left(S_{xx} \frac{d\psi_i^{(2)}}{dx} \psi_j^{(3)} + B_{xx} \frac{dw}{dx} \frac{d\psi_i^{(2)}}{dx} \frac{d\psi_j^{(3)}}{dx} \right) dx \tag{24}$$

$$K_{ij}^{32} = \int_{x_a}^{x_b} \left(S_{xx} \psi_i^{(3)} \frac{d\psi_j^{(2)}}{dx} + \frac{1}{2} B_{xx} \frac{dw}{dx} \frac{d\psi_i^{(3)}}{dx} \frac{d\psi_j^{(2)}}{dx} \right) dx \tag{25}$$

$$K_{ij}^{33} = \int_{x_a}^{x_b} \left(D_{xx} \frac{d\psi_i^{(3)}}{dx} \frac{d\psi_j^{(3)}}{dx} + S_{xx} \psi_i^{(3)} \psi_j^{(3)} \right) dx \tag{26}$$

and the force coefficients are

$$\begin{aligned} F_i^1 &= \int_{x_a}^{x_b} \psi_i^{(1)} f dx + Q_1^e \psi_i^{(1)}(x_a) + Q_4^e \psi_i^{(1)}(x_b) \\ F_i^2 &= \int_{x_a}^{x_b} \psi_i^{(2)} q dx + Q_2^e \psi_i^{(2)}(x_a) + Q_5^e \psi_i^{(2)}(x_b) \\ F_i^3 &= Q_3^e \psi_i^{(3)}(x_a) + Q_6^e \psi_i^{(3)}(x_b) \end{aligned} \tag{27}$$

The nonlinearity of the problem can be seen through the stiffness coefficients in Eq (20) it is necessary to know the displacement field, as some stiffness coefficient terms depend on the nodal values of the displacements or the slopes. The non-linear resulting equation will be solved using Newton's Method.

2.3 Shear and Membrane Locking

The simplest Timoshenko beam finite element uses linear interpolation of both transverse deflection w and rotation ϕ_x (Reddy, 2014). For thin beams, with large ratios of length to thickness, we have that the slope of the deflection dw/dx should be equal to $-\phi_x$. When we adopt the linear approximation dw/dx is constant, while ϕ_x is linear, this terms have different polynomial degrees, so they can't be equal. This inconsistency results in zero displacements and rotations, which trivially satisfy $dw/dx = -\phi_x$. This numerical problem is known as *shear locking*. So we should follow

$$\text{(shear strain)} \quad \gamma_{xz}^0 \equiv \phi_x + \frac{dw}{dx} = \text{constant} \tag{28}$$

However considering the rotation constant is not admissible because the bending energy of the element would be zero, represented by Eq. (29).

$$\int_{x_a}^{x_b} D_{xx} \frac{1}{2} \left(\frac{d\phi_x}{dx} \right)^2 dx \tag{29}$$

There is another inconsistency in the formulation, created by the coupling of the axial u and transverse w displacements introduced by the *von Kármán nonlinearity*. To illustrate the problem we can analyze a hinged-hinged beam with a transverse loading. A hinge does not restrict axial displacement so we have that the beam is free to slide and its axial strain should be zero. However using same degree (m) interpolation of axial u and transverse w displacements does not allow for the membrane strain terms to cancel out

$$\text{(membrane strain)} \quad \varepsilon^0_{xx} \equiv \frac{du}{dx} + \frac{1}{2}\left(\frac{dw}{dx}\right)^2 = 0 \tag{30}$$

it can be seen that du/dx would be $(m-1)$, while $(dw/dx)^2$ would be $(m-2)$. Because the membrane strain terms are non-zero the stiffness of the beam increases reducing the deflection, this numerical problem is know as *membrane locking*.

We then have from Equations (28) and (30) two constraints that must be satisfied

$$\phi_x \sim \frac{dw}{dx} \qquad\qquad \frac{du}{dx} \sim \left(\frac{dw}{dx}\right)^2 \tag{31}$$

the similarity in Eq. (31) means that the terms must have same degree of polynomial variation. To solve this constraints there are two main procedures: *Consistent interpolation* in which the degree of approximation for the displacements is chosen so it satisfies Eq. (31), this creates a stiffness matrix with different degrees of freedom at different nodes, making it difficult to implement on a computer program and *Reduced Integration* in which all displacements and rotations are approximated with same degree interpolation, but selective numerical reduced integration is used to satisfy Eq. (31).

We shall use here the reduced integration method, this means that the integration will be conducted using less points to integrate the associated shear and nonlinear terms, reducing their polynomial degree and thus satisfying the constraints.

2.4 Newton's Method

Numerical procedures used to solve nonlinear equations are iterative by nature. They are based on the linearization of the stiffness matrix $\mathbf{K}$. The element equations are then assembled and the boundary conditions are imposed before using the procedure (Reddy, 2014). In this paper we will use the Newton's Iteration Procedure, because of the iterative nature of the procedure it is necessary to solve the problem first before starting it. The first solution is normally given by the linear problem as

$$\mathbf{U}^{(1)} = [\mathbf{K}^{(0)}(\mathbf{U}^{(0)})]^{-1}\mathbf{F}^{(0)} \tag{32}$$

where the solution vector $\mathbf{U}^{(0)}$ is composed by zeros. Then we define the residual vector $\mathbf{R}$

$$\mathbf{R}^{(r)} \equiv \mathbf{K}^{(r)}\mathbf{U}^{(r)} - \mathbf{F}^{(r)} \tag{33}$$

where the index (r) represents, the current iteration. This will be used on the formulation of the method and can be used to check the solution, when its value reaches an established tolerance the solution has converged.

We then expand the residual vector in Taylor's series about the known solution $\mathbf{U}^{(r-1)}$ of the last iteration

$$\mathbf{R}^{(r)} = \mathbf{R}^{(r-1)} + \left(\frac{\partial \mathbf{R}}{\partial \mathbf{U}}\right)^{(r-1)} \Delta\mathbf{U} + ... \tag{34}$$

where

$$\Delta\mathbf{U} = \mathbf{U}^{(r)} - \mathbf{U}^{(r-1)} \tag{35}$$

then by neglecting the second order and higher terms in $\Delta\mathbf{U}$ and setting $\mathbf{R}^{(r)}$ as zero, we obtain

$$\left(\frac{\partial \mathbf{R}}{\partial \mathbf{U}}\right)^{(r-1)} \Delta\mathbf{U} = -\mathbf{R}^{(r-1)} \tag{36}$$

We then define the Tangent matrix $\mathbf{T}$ as

$$\mathbf{T}^{(r-1)} \equiv \left(\frac{\partial \mathbf{R}}{\partial \mathbf{U}}\right)^{(r-1)} \tag{37}$$

The Eq.(37) can be solved for the Timoshenko formulation

$$T^{\alpha\beta}_{ij} = K^{\alpha\beta}_{ij} + \sum_{\gamma=1}^{3}\sum_{k=1}^{n} \frac{\partial}{\partial \Delta^{\beta}_{j}}\left(K^{\alpha\gamma}_{ik}\right)\Delta^{\gamma}_{k} - \frac{\partial F^{\alpha}_{i}}{\partial \Delta^{\beta}_{j}} \tag{38}$$

$$\mathbf{T}^{\alpha 1} = \mathbf{K}^{\alpha 1}, \quad \mathbf{T}^{\alpha 3} = \mathbf{K}^{\alpha 3} \text{ para } \alpha = 1, 2, 3; \quad \mathbf{T}^{12} = 2\mathbf{K}_{ij}^{12}, \quad \mathbf{T}^{32} = \mathbf{K}_{ji}^{23} \tag{39}$$

$$T_{ij}^{22} = K_{ij}^{22} + \int_{x_a}^{x_b} \left\{ A_{xx} \left[\frac{du}{dx} + \left(\frac{dw}{dx} \right)^2 \right] + B_{xx} \frac{d\phi_x}{dx} \right\} \frac{d\psi_i^{(2)}}{dx} \frac{d\psi_j^{(2)}}{dx} dx \tag{40}$$

with the residual vector and tangent matrix in hands we can finally obtain the solution of the current iteration as

$$\Delta \mathbf{U} = -\mathbf{T}^{-1}\mathbf{R} \Rightarrow \mathbf{U}^r = \mathbf{U}^{(r-1)} + \Delta \mathbf{U} \tag{41}$$

At the end of each iteration of the procedure we check for the convergence of the solution by comparing the current solution to the last in a Euclidean norm. The norm has to be lesser than or equal to a tolerance value ϵ previously determined, as represented on Eq. (42). The iteration process continues until the condition is met, or a maximum limit of iterations is reached.

$$\sqrt{\frac{\Delta \mathbf{U} \Delta \mathbf{U}}{\mathbf{U}^{(r)} \mathbf{U}^{(r)}}} = \sqrt{\frac{\sum_{I=1}^{N} |U_I^{(r)} - U_I^{(r-1)}|^2}{\sum_{I=1}^{N} |U_I^{(r)}|}} \leq \epsilon \tag{42}$$

2.5 Functionally Graded Material

For this paper two types of functionally graded materials (FGM) functions will be evaluated for the formulation of the beams. One of them is given by Eq. (43), which describes a beam whose top surface is 100% material 1 and its bottom surface 100% material 2

$$E(x, z) = [E_1(x) - E_2(x)]\, f(z) + E_2(x), \quad f(z) = \left(\frac{1}{2} + \frac{z}{H} \right)^n \tag{43}$$

where $E_1(x)$ and $E_2(x)$ represents the elastic modulus of the two materials being combined, H is the thickness of the beam, $f(z)$ is a function that dictates the volume fraction of material 1 and n is the power-law index of the function $f(z)$. When $n = 0$ the beam is fully composed of material 1 and when n is a large number the beam is composed solely of material 2, as can be observed in Figure (2a).

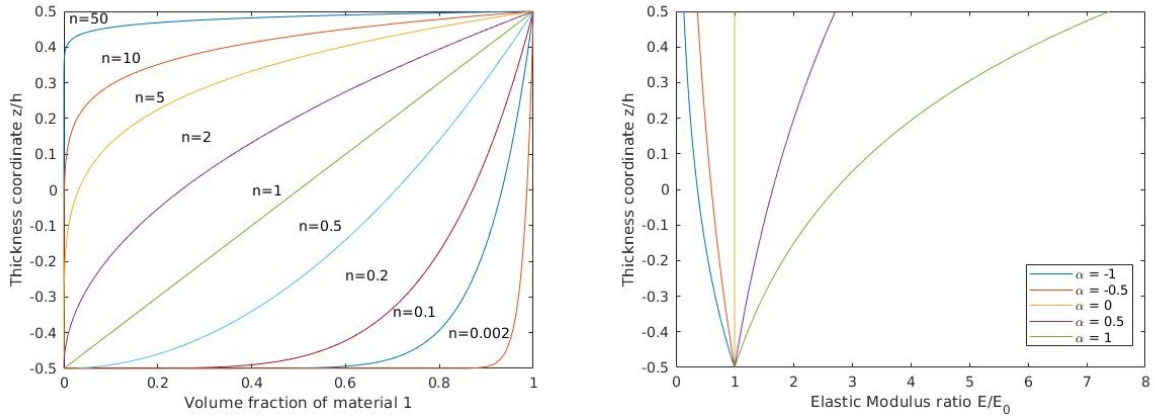

Figure 2. (a) Volume fraction of material 1 as a function of the power-law index n; (b) Elastic modulus ratio as a function of the exponential index α.

The other material distribution that is going to be analyzed for beams is the exponential distribution given by

$$E(z) = E_0 e^{2\alpha(z + H/2)} \tag{44}$$

here E_0 is the elastic modulus at the bottom surface of the beam and α is the coefficient that controls its exponential behaviour, as illustrated by Figure (2b).

3. RESULTS

The formulation developed on the last section was used to implement a FEM algorithm using the Matlab ® software. To evaluate the algorithm we will use four numerical problems that are presented on the subsequent subsections.

3.1 Numerical Example 1

This Example was proposed by Reddy (2014). We have a functionally graded beam, which elastic modulus is given by Eq. (43), of length $L = 2.54$ m, height $H = 2.54$ cm and width $B = 2.54$ cm. This beam is fixed at the left end and pinned at the right end, subjected to an uniformly distributed load q_0, as represented by Figure (3). The material properties of the beam are: $E_1 = 206.84$ GPa, $E_2 = 68.95$ GPa, Poisson coefficient $\nu = 0.3$ and $K_s = 5/6$. We solved this problem using eight linear Timoshenko beam elements, three different values of $n = [0, 1, 10]$, a tolerance value $\epsilon = 10^{-3}$ and a load increment of $\Delta q_0 = 42.71$ N/m. The increment load is used for a better convergence of the solution, basically we solve the problem for a small load and use this solution to solve the next iteration while linearly increasing the load until it reaches the desired value.

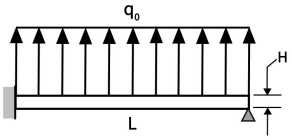

Figure 3. Example 1.

In order to better analyze the results we represented the solution of the problem in Figure (4a) by the deflection $w(x)$ of the beam at $x = L/2$.

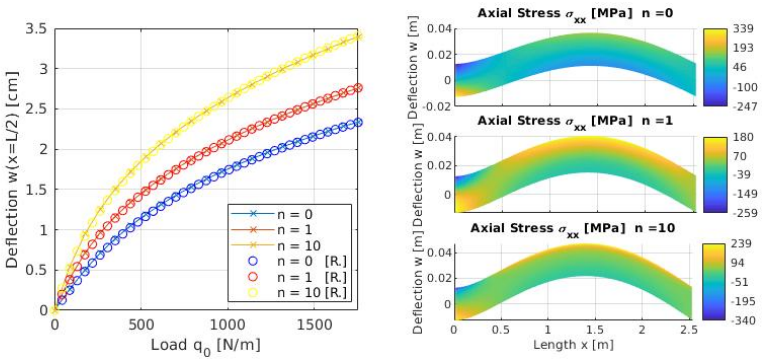

Figure 4. (a) Deflection at the middle of the beam as a function of the distributed load, where the circles represent Reddy's (2014) results; (b) Axial stress field for each value of n.

The results were compared to the ones obtained by Reddy (2014) to validate the algorithm. The graph represented on Fig. (4a) shows us the nonlinearity of the formulation. The deflection at $x = L/2$ varies nonlinearly, because of the increase in stiffness of the beam created by the u and w coupled terms. It can also be observed the effect of the volume fraction of each material on the stiffness of the beam, since material 1 has a bigger modulus of elasticity the beam with $n = 0$ is the most rigid and increasing this term causes a larger deflection. In order to analyze the behavior of the stress on the beam, the stress field was plotted. The graph represented at Fig. (4b) demonstrates that at first, raising the volume fraction of material 2 reduces the stress concentration at the bottom of the clamped side of the beam and intensifies it at the top, increasing it further causes the stress concentration on both ends to increase. This is caused by both the deflection increase and the material disposition through the beam's thickness as can be seen on Figure (2a).

The same problem can be modified to study the behavior of the exponential FGM. The alteration on the material properties were: $E_0 = 70$ GPa and $\alpha = [-20, 10, 30]$. The solution of the problem is represented at Figure (5). Negative values of α reduce the elastic modulus through the beam, while positive values increase it. This behavior can be identified on Fig. (5a), as the beam hardens the deflection decreases. The nonlinear variation of the deflection can also be seen in this beam. The Figure (5b) shows the axial stress field of the beam for different α values, at first the stress concentration decreases as the beam hardens, but for higher α values the exponential behavior of the material distribution is stronger causing a bigger difference between the bottom and top surface, as shown by Fig (2b), which leads to a larger stress concentration at the top surface of the beam.

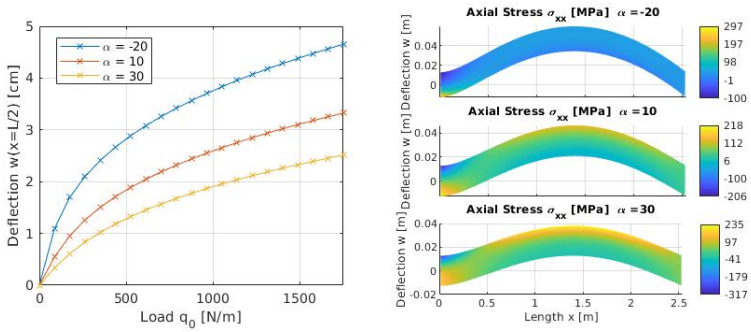

Figure 5. (a) Deflection at the middle of the beam as a function of the distributed load; (b) Axial stress field for each value of α.

3.2 Numerical Example 2

This next example will be used to validate the algorithm for a beam with exponential functionally graded material. Its elastic modulus is given by Eq. (44). As a first validation for the model, we will be neglecting the nonlinear part of the algorithm and compare the linear results to an analyses made using 2D plane stress state elements in Ansys. ®. We have a beam of length $L = 50$ cm, height $H = 10$ cm and width $B = 10$ cm. This beam is fixed at both ends, subjected to an uniformly distributed load $q_0 = 10000$ kN/m, as represented by Figure (6). The material properties of the beam are: $E_0 = 70$ GPa, $\alpha = 4$, Poisson coefficient $\nu = 0.3$ and $K_s = 5/6$.

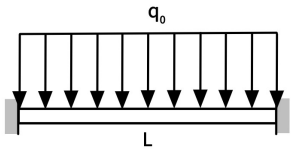

Figure 6. Example 2.

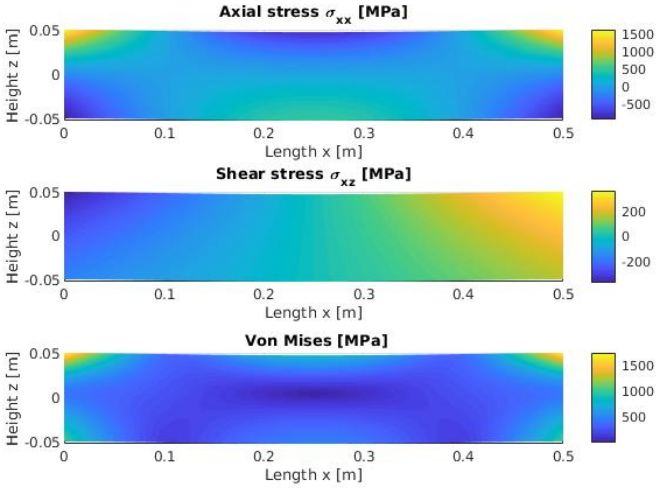

Figure 7. Stress field for the Example 2.

At Fig. (7) we can see the stress field caused by the load q_0. The main difference between both solutions obtained is observed at the edges of the beam, because of the stress concentration experienced by the 2D element at its edges. So in order to analyze the results far from the edges the graphs represented by Fig. (8) were made. As we can see the results at $z = 0$, and at $x = L/2$ are satisfactory. The main source of divergence is the way the Ansys model was build, the beam was divided in 10 and each part was assigned a mean elastic modulus to represent the functionally graded material.

The Timoshenko theory predicts a constant shear stress along the beam's thickness. Hence, a comparison with the 2D elasticity theory, which is a distorted parabolical distribution for the exponentially graded beam, is not feasible.

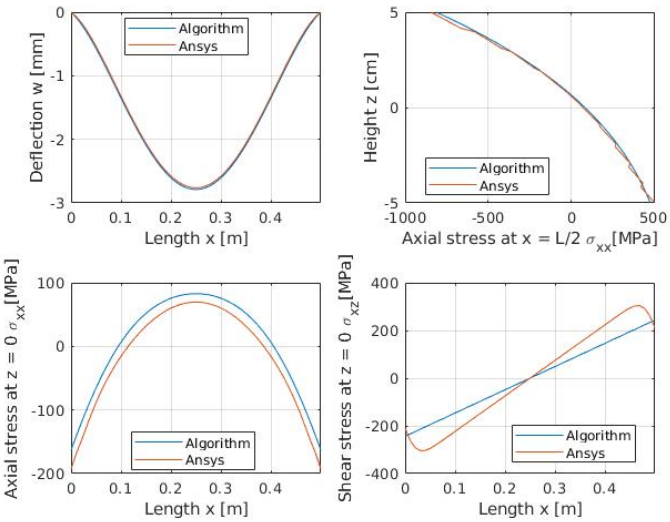

Figure 8. Results at the center line and middle of the beam.

3.3 Numerical Example 3

The third example is centered on the different type of fixations of the beam. For this analysis a beam with the properties: $L = 90$ cm, $H = B = 3$ cm, $E = 200$ GPa, $\nu = 0.3$ and $K_s = 5/6$, submitted to increments of $\Delta q_0 = -100$ N/m and a tolerance value $\epsilon = 10^{-3}$, will be used, while the fixation at both ends is varied. The results represented by

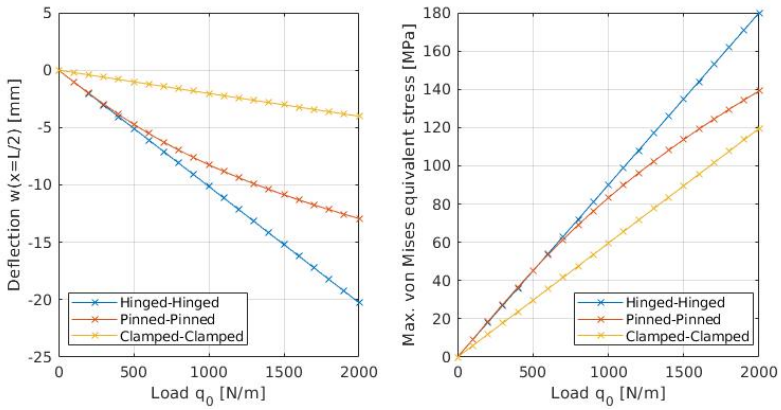

Figure 9. (a) Deflection at the middle of the beam for 3 fixations; (b) Maximum von Mises equivalent stress of the beam for 3 fixations.

Figure (9) validate the use of reduced integration to prevent Membrane Locking. The hinged-hinged beam presents a linear behavior, since it has no axial restrictions as discussed before. The pinned-pinned beam shows a non-linear effect for the deflection and stress and the clamped-clamped beam shows a linear relation, because of its large stiffness value.

3.4 Numerical Example 4

The fourth example is centered on the length-to-height ratio of a clamped-clamped beam. For this analysis a beam with the properties: $H = B = 3$ cm, $E = 200$ GPa, $\nu = 0.3$ and $K_s = 5/6$, submitted to increments of $\Delta q_0 = -100$ N/m and a tolerance value $\epsilon = 10^{-3}$, will be used, while the L/H ratio is varied. The dimensionless deflection given by $w_b = w(x = L/2) * H^2/L^3$ will be used to compare the results. The results represented on Figure (10a) show us that the clamped-clamped beam starts presenting nonlinear behavior at high length-to-height ratios. Figure (10a) also validates the use of the reduced integration on preventing Shear Locking, for large L/H ratios the beam doesn't experience zero displacements and as represented by Figure (10b) the shear stress becomes negligible when compared to the axial stress.

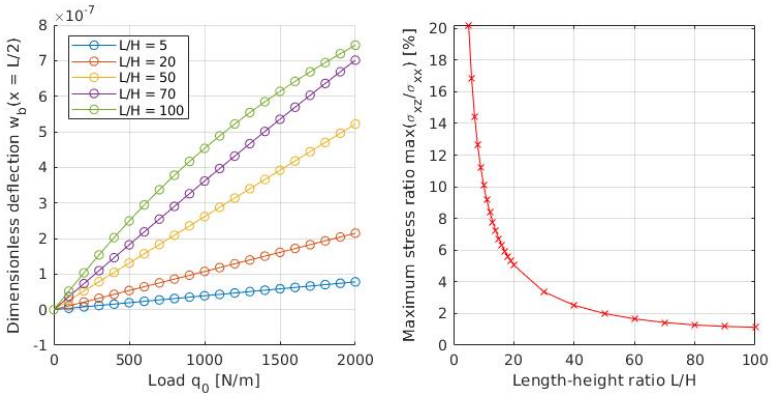

Figure 10. Results at the center line and middle of the beam.

4. CONCLUSION

We implemented here a non-linear geometric FEM formulation for functionally graded timoshenko beams. Reduced integration successfully prevents shear and membrane locking effects. We presented results for power and exponential laws graded materials. After analyzing both material it is clear that not only the mean value of elastic modulus of each beam plays an important role on the deflection and concentration of stress, but also the rate of hardening and softening. Since the problem is nonlinear the use of these materials requires a study of the influence that both factors have on the desired result.

5. REFERENCES

Dym, Clive L., and Irving H. Shames. Solid mechanics : a variational approach. New York London: Springer, 2013.

Reddy, J. N. An introduction to the finite element method. New York, NY: McGraw-Hill Higher Education, 2006.

Reddy, J. N. An introduction to nonlinear finite element analysis : with applications to heat transfer, fluid mechanics, and solid mechanics. Oxford: Oxford University Press, 2014.

SURESH, S. e MORTENSEN, A. Fundamentals of Functionally Graded Materials. Institute of Materials IOM Communications, London, 1998.

6. RESPONSIBILITY NOTICE

The authors are solely responsible for the printed material included in this paper.